PCCP

Accepted Manuscript




ROYAL SOCIETY OF CHEMISTRY

www.rsc.org/pccp

Physical Chemistry Chemical Physics
CREATED USING THE RSC LaTeX PCCP ARTICLE TEMPLATE – SEE www.rsc.org/electronicfiles FOR DETAILS
ARTICLE TYPE www. rsc.org/xxxxxx | XXXXXXXX

# Can the current density map topology be extracted from the nucleus independent chemical shifts ?

**Sofie Van Damme[a,b], Guillaume Acke [a,b], Remco W.A. Havenith[a,b,c] and Patrick Bultinck*[a,b]**

***Received Xth XXXXXXXXXX 20XX, Accepted Xth XXXXXXXXX 20XX***
***First published on the web Xth XXXXXXXXXX 200X***
**DOI: 10.1039/b000000x**

Aromatic compounds are characterised by the presence of a ring current when in a magnetic field. As a consequence, current density maps are used to assess (the degree of) aromaticity of a compound. However, often a more discrete set of so-called Nucleus Independent Chemical Shift (NICS) values is used that is derived from the current density. It is shown here that there is no simple one-to-one relationship that allows reconstructing current density maps from only NICS-values. NICS values should therefore not be used as aromaticity indices without analysis of the ab initio computed current density map.

## 1 Introduction

One of the most enigmatic molecules in chemistry is without any doubt benzene. Faraday described the discovery of benzene at a meeting of the Royal Society on June 16, 1825 where his paper described the separation of this hydrocarbon from a complex mixture, the study of its properties, and the determination of its composition [1,2]. No structure was revealed yet and this remained the case until Kekulé joined Ghent University in 1858. During his previous appointment in Heidelberg, Kekulé had already proven the tetravalence of carbon [3] and much of his work at Ghent University continued to focus on the structure of (organic) compounds, leading eventually to the cyclic structure of benzene [4,5]. In this sense, Kekulé can be properly considered the founding father of structural organic chemistry. Up to this day, benzene not only occurs in many chemicals on which the wealth and health of our current society depends, the resolution of its structure in many ways revolutionised much of structural chemistry and set the benchmark for both theoretical as well as experimental work in the field known as aromaticity. Despite the importance of aromatic compounds, the very nature of aromaticity is rather poorly defined quantum mechanically [6]. Different criteria are often used to identify and quantify aromatic character : energetic [7], magnetic [8–11], structural [12] and electronic [13–18]. However, in many cases not all four criteria lead to the same conclusion [7,19–24] and any conclusion on a molecule being aromatic or not risks to be biased by the chemist's preference on what the most important aromaticity indicator is. A rather popular criterion is the magnetic criterion based on the old observation by London [25] that an unsaturated ring can sustain an induced ring current in the presence of a uniform magnetic field perpendicular to the molecular plane. The basic implication here is that aromaticity is equivalent to cyclic delocalisation and the mobility of $\pi$-electrons giving rise to a diamagnetic current.The calculation of ring current density was further made possible thanks to many excellent contributions such as that of Pople [26], Keith and Bader [27].

Nowadays, the induced ring current in (anti)aromatic systems may be evaluated directly with current density analysis methods as in references [28,29] or indirectly by evaluating observables such as proton chemical shifts that are then explained in terms of the underlying current density [30]. Chemical shifts have long been used as indirect indicators of aromaticity, e.g., in fullerenes [31]. Different probes have been used to such ends, including encapsulated $^3$He or $Li^+$. In 1996, Schleyer et al. [8] introduced absolute magnetic shieldings at ring centres as an aromaticity criterion. The Nucleus Independent Chemical Shifts, or NICS value, at some point **r** corresponds to the average of the diagonal elements of the nuclear shielding tensor at this point. Computing NICS in a single point and using it as a measure of the strength and direction of the ring current and assuming all information of the ring current in the entire molecule is reflected in one single measure met significant criticism [32–34] and later work led to a fairly wide set of rules on where to compute NICS values, with NICS values computed 1 Bohr or 1 Å above the centre of the ring as one of the main locations [35,36]. To no small extent thanks to its ease for calculation, the NICSs have become part of the standard toolbox of computational chemists although any analysis has to be made with great care [9,37]. The problem remains that NICSs are not current densities but derived quantities and, as mentioned above, the distinguishing characteristic of an aromatic system

[a] *Ghent University, Faculty of Science, Department of Inorganic and Physical Chemistry, Krijgslaan 281, S3, 9000 Ghent, Belgium*
[b] *Members of the QCMM Alliance Ghent-Brussels*
[c] *Theoretical Chemistry, Zernike Institute for Advanced Materials and Stratingh Institute for Chemistry, University of Groningen, 9747 AG Groningen, The Netherlands.*

in the ring current. Although a ring current will lead to a specific NICS signature in the chosen point(s) the emphasis of the present paper lies on the question whether a specific NICS signature can *automatically* be considered proof of a current density. As will become clear below, an integral is evaluated involving the current density but from a limited discrete set of NICS values one cannot *per se* reconstruct the integrand. Since magnetic shielding is proportional to the third power of the distance of electrons from the probe, it does not reflect all points around it to equal extent. In order to alleviate this criticism, methods such as the NICS-scan[38], 2 dimensional NICS scans[39] or 3-dimensional NICS visualisations[40,41] or analogues[42] have been introduced. Still, the fact remains that the current density distribution determines the nuclear shielding tensors at any point in space but the converse is not necessarily true: the value of the induced magnetic field at one point $\mathbf{r}$ could originate from a number of significantly different distributions of currents. Again here, several studies have tried to relieve this problem, such as the ARCS method[43] and its refinements[44] or the series of classical models invoked by Pelloni et al[45–47].

The aim of the present paper is to examine carefully whether one can, in a robust manner, extract information on the current density from (a set of) NICS value(s) or whether one should simply always compute the current density map itself. The method used will be loosely based on reversed engineering. Instead of generating NICS out of current densities, we will try to generate current densities out of one or a finite number of NICS values. Therefore, several types of sets of NICS values will be investigated for their ability to generate a current density map, and the stability of the resulting current density map will be the subject of this research. The reader will immediately see a parallel with reducing a molecular electrostatic potential to a set of point charges. There too, an entire field is related to a discrete set of points and it is well-known that many problems of statistical nature also occur[48].

## 2 Theory

A current density in a molecule gives rise to a magnetic field that affects the long range shielding of any probes. When a molecule is placed in an external magnetic field, $\mathbf{B}_0$, local magnetic fields are induced which reduce (shield) or increase (deshield) the net magnetic fields at the nuclear sites. The magnitude of the induced local field depends on the nature of the nucleus, the electronic structure of the molecule as well as the orientation of the molecule with respect to $\mathbf{B}_0$. The induced magnetic field ($\mathbf{B}^{\text{ind}}$) can be computed from the induced current density of the molecule ($\mathbf{J}$) using the Biot-Savart law[49]. According to this law, a current element $\mathbf{dI}(\mathbf{r})$ at $\mathbf{r}$ creates a magnetic field $\mathbf{B}^{\text{ind}}$ at position $\mathbf{r_R}$ as in equation 1.

$$\mathrm{d}\mathbf{B}^{\text{ind}}(\mathbf{r_R}) = \frac{\mu_0}{4\pi}\frac{\mathrm{d}\mathbf{I}(\mathbf{r}) \times \widehat{(\mathbf{r_R}-\mathbf{r})}}{|\mathbf{r_R}-\mathbf{r}|^2} \tag{1}$$

With $\widehat{(\mathbf{r_R}-\mathbf{r})}$ the unit vector of $(\mathbf{r_R}-\mathbf{r})$, the vector from the current element to the point $\mathbf{r_R}$. The constant $\mu_0$ is known as the permeability of free space $\mu_0 = 4\pi \times 10^{-7}$ Hm$^{-1}$.
In particular, if the current element comes from a bulk current density, as the current generated by an external magnetic field $\mathbf{B}^{\text{ext}}$, $\mathrm{d}\mathbf{I}(\mathbf{r})$ becomes $\mathbf{J}^B(\mathbf{r})\mathrm{d}^3\mathbf{r}$, with $\mathbf{J}^B$ the induced current density.

$$\mathrm{d}\mathbf{B}^{\text{ind}}(\mathbf{r_R}) = \frac{\mu_0}{4\pi}\frac{\mathbf{J}^B(\mathbf{r}) \times \widehat{(\mathbf{r_R}-\mathbf{r})}}{|\mathbf{r_R}-\mathbf{r}|^2}\mathrm{d}^3\mathbf{r} \tag{2}$$

The induced magnetic field $\mathbf{B}^{\text{ind}}$ at point $\mathbf{r_R}$ is obtained through the integration over $\mathbb{R}^3$.

$$\mathbf{B}^{\text{ind}}(\mathbf{r_R}) = \frac{\mu_0}{4\pi}\int_{\mathbb{R}^3}\frac{\mathbf{J}^B(\mathbf{r}) \times \widehat{(\mathbf{r_R}-\mathbf{r})}}{|\mathbf{r_R}-\mathbf{r}|^2}\mathrm{d}^3\mathbf{r} \tag{3}$$

Discretisation of the Biot-Savart law involves an approximation of $\mathrm{d}\mathbf{B}^{\text{ind}}$ by $\Delta\mathbf{B}^{\text{ind}}$, where the displacement vector is now calculated from the centre coordinates of the discretised segment, small enough to apply the approximation, with volume $\Delta^3\mathbf{r_b}$, located at $\mathbf{r_b}$

$$\Delta\mathbf{B}^{\text{ind}}_b(\mathbf{r_R}) = \frac{\mu_0}{4\pi}\frac{\mathbf{J}^B(\mathbf{r_b}) \times \widehat{(\mathbf{r_R}-\mathbf{r_b})}}{|\mathbf{r_R}-\mathbf{r_b}|^2}\Delta^3\mathbf{r_b} \tag{4}$$

The induced magnetic field $\mathbf{B}^{\text{ind}}$ is calculated by adding together the contributions from each discretised segment.

$$\mathbf{B}^{\text{ind}}(\mathbf{r_R}) = \sum_{b=1}^{N_b}\frac{\mu_0}{4\pi}\frac{\mathbf{J}^B(\mathbf{r_b}) \times (\mathbf{r_R}-\mathbf{r_b})}{|\mathbf{r_R}-\mathbf{r_b}|^3}\Delta^3\mathbf{r_b} \tag{5}$$

Defolding the tensor product, equation 6,

$$\mathbf{J}^B(\mathbf{r_b}) \times (\mathbf{r_R}-\mathbf{r_b}) = \begin{vmatrix} \mathbf{i} & \mathbf{j} & \mathbf{k} \\ J^B_x(\mathbf{r_b}) & J^B_y(\mathbf{r_b}) & J^B_z(\mathbf{r_b}) \\ x_R - x_b & y_R - y_b & z_R - z_b \end{vmatrix} \tag{6}$$

enables us to find an expression for the individual $x$, $y$ and $z$-terms of the induced magnetic field $\mathbf{B}^{\text{ind}}$ at a point $\mathbf{r_R}$ in space.

$$\mathbf{B}^{\text{ind}}(\mathbf{r_R}) = B^{\text{ind}}_x(\mathbf{r_R})\mathbf{i} + B^{\text{ind}}_y(\mathbf{r_R})\mathbf{j} + B^{\text{ind}}_z(\mathbf{r_R})\mathbf{k} \tag{7}$$

For $B^{\text{ind}}_z$, one finds equation 8. Analogues expressions are found for $B^{\text{ind}}_x$ and $B^{\text{ind}}_y$

$$B^{\text{ind}}_z(\mathbf{r_R}) = \frac{\mu_0}{4\pi}\sum_{b=1}^{N_b}\frac{\Delta^3\mathbf{r_b}}{|\mathbf{r_R}-\mathbf{r_b}|^3}\left[J_x(\mathbf{r_b})(y_R - y_b) - J_y(\mathbf{r_b})(x_R - x_b)\right] \tag{8}$$

The magnetic shielding tensor field $\boldsymbol{\sigma}(\mathbf{r_R})$, can be computed directly from these quantities. It is important to note that equation 8 does not contain information about a nucleus, and thus, the shielding tensor can be computed at any place in space; i.e. at the position of the nucleus or somewhere else. Hence, the magnetic shielding tensor $\boldsymbol{\sigma}(\mathbf{r_R})$ is a generalisation of the magnetic shielding tensor of NMR spectroscopy to an arbitrary point $\mathbf{r_R}$ in space. The induced magnetic field $\mathbf{B}^{\text{ind}}(\mathbf{r_R})$ is related with the shielding tensor field at position $\mathbf{r_R}$ and the external magnetic field $\mathbf{B}^{\text{ext}}$, assumed uniform.

$$\mathbf{B}^{\text{ind}}(\mathbf{r_R}) = -\boldsymbol{\sigma}(\mathbf{r_R})\mathbf{B}^{\text{ext}} \tag{9}$$

The shielding tensor describes the magnitude and orientation dependence of the magnetic shielding and can be represented in a $3 \times 3$ matrix, in 3D Cartesian space.

$$\begin{bmatrix} \sigma_{xx}(\mathbf{r_R}) & \sigma_{xy}(\mathbf{r_R}) & \sigma_{xz}(\mathbf{r_R}) \\ \sigma_{yx}(\mathbf{r_R}) & \sigma_{yy}(\mathbf{r_R}) & \sigma_{yz}(\mathbf{r_R}) \\ \sigma_{zx}(\mathbf{r_R}) & \sigma_{zy}(\mathbf{r_R}) & \sigma_{zz}(\mathbf{r_R}) \end{bmatrix} \tag{10}$$

Each element $\sigma_{ij}$, represents the $i$th component of the shielding when $\mathbf{B}^{\text{ext}}$ is applied along the $j$-axis. Obviously magnetic properties are physical quantities and depend on the orientation of the molecules relative to the applied magnetic field. The initial depiction of induced magnetic fields (surrounding benzene in the case of Pople[26]) is based on the assumption that the external magnetic field is applied in the direction perpendicular to the molecular plane. Putting the molecule in the $xy$-plane and assuming that the uniform magnetic field is applied pointing in the $-z$ direction, with a magnitude of $B^{\text{ext}}$ (unit Tesla), $\mathbf{B}^{\text{ext}} = 0\mathbf{i} + 0\mathbf{j} - B^{\text{ext}}\mathbf{k}$. The induced magnetic field, equation 10 can now be defined as equation 11

$$\begin{bmatrix} B_x^{\text{ind}}(\mathbf{r_R}) \\ B_y^{\text{ind}}(\mathbf{r_R}) \\ B_z^{\text{ind}}(\mathbf{r_R}) \end{bmatrix} = - \begin{bmatrix} \sigma_{xx}(\mathbf{r_R}) & \sigma_{xy}(\mathbf{r_R}) & \sigma_{xz}(\mathbf{r_R}) \\ \sigma_{yx}(\mathbf{r_R}) & \sigma_{yy}(\mathbf{r_R}) & \sigma_{yz}(\mathbf{r_R}) \\ \sigma_{zx}(\mathbf{r_R}) & \sigma_{zy}(\mathbf{r_R}) & \sigma_{zz}(\mathbf{r_R}) \end{bmatrix} \begin{bmatrix} 0 \\ 0 \\ -B^{\text{ext}} \end{bmatrix} \tag{11}$$

Due to the choice in the external field, an expression for the last column elements of the tensor can be found.

$$B_x^{\text{ind}}(\mathbf{r_R}) = \sigma_{xz}(\mathbf{r_R}) \cdot B^{\text{ext}} \tag{12}$$

$$B_y^{\text{ind}}(\mathbf{r_R}) = \sigma_{yz}(\mathbf{r_R}) \cdot B^{\text{ext}} \tag{13}$$

$$B_z^{\text{ind}}(\mathbf{r_R}) = \sigma_{zz}(\mathbf{r_R}) \cdot B^{\text{ext}} \tag{14}$$

The expressions for the elements in the last column of the tensor expression, $\sigma_{iz}$, are for example for $\sigma_{zz}$ given in equation 15.

$$\sigma_{zz}(\mathbf{r_R}) \equiv \frac{1}{B^{\text{ext}}} \frac{\mu_0}{4\pi} \sum_{b=1}^{N_b} \frac{\Delta^3 r_b}{|\mathbf{r_R} - \mathbf{r_b}|^3} \left[ J_x(\mathbf{r_b})(y_R - y_b) - J_y(\mathbf{r_b})(x_R - x_b) \right] \tag{15}$$

Given the expressions for $\sigma_{iz}$, the equation as in 15 can be solved using matrix expression equation 16

$$\begin{matrix} \boldsymbol{\sigma} \\ \begin{bmatrix} \boldsymbol{\sigma}_{\text{xz}} \\ \boldsymbol{\sigma}_{\text{yz}} \\ \boldsymbol{\sigma}_{\text{zz}} \end{bmatrix} \end{matrix} = \frac{1}{B^{\text{ext}}} \frac{\mu_0}{4\pi} \begin{matrix} \mathbf{C} \\ \begin{bmatrix} \mathbf{0} & \mathbf{Z} & -\mathbf{Y} \\ -\mathbf{Z} & \mathbf{0} & \mathbf{X} \\ \mathbf{Y} & -\mathbf{X} & \mathbf{0} \end{bmatrix} \end{matrix} \begin{matrix} \mathbf{J} \\ \begin{bmatrix} \mathbf{J}_{\text{x}} \\ \mathbf{J}_{\text{y}} \\ \mathbf{J}_{\text{z}} \end{bmatrix} \end{matrix} \tag{16}$$

Where $\boldsymbol{\sigma}_{(\text{x,y,z})\text{z}}$ constitute the column vector $\boldsymbol{\sigma}$, gathering $3N$ $\sigma_{iz}(\mathbf{r_R})$ values assuming $N$ sampling points $\mathbf{r_R}$. This vector will be referred to as the shielding vector, implying the collection of the tensor values in the $x$, $y$, $z$ direction as an answer to a magnetic field applied in the $z$-direction. $\mathbf{J}_{(\text{x,y,z})}$ are the building blocks of the column vector $\mathbf{J}$ with $3N_b$ elements for the current density vector components, $J_x(\mathbf{r_b})$, $J_y(\mathbf{r_b})$ and $J_z(\mathbf{r_b})$. The coordinate matrix $\mathbf{C}$ is constructed out of the matrices $\mathbf{X}, \mathbf{Y}$ and $\mathbf{Z}$ of dimensions $N \times N_b$, as for example for $\mathbf{Z}$, equation 17

$$\mathbf{Z} = \begin{bmatrix} \frac{(z_R(1) - z_b(1))}{|\mathbf{r_R}(1) - \mathbf{r_b}(1)|^3} & \cdots & \frac{(z_R(1) - z_b(N_b))}{|\mathbf{r_R}(1) - \mathbf{r_b}(N_b)|^3} \\ \vdots & \ddots & \vdots \\ \frac{(z_R(N) - z_b(1))}{|\mathbf{r_R}(N) - \mathbf{r_b}(1)|^3} & \cdots & \frac{(z_R(N) - z_b(N_b))}{|\mathbf{r_R}(N) - \mathbf{r_b}(N_b)|^3} \end{bmatrix} \tag{17}$$

Matrix equation 16 can be solved for the current density values on the chosen grid, assumed that one has the shielding tensor values.

NICS$(\mathbf{r_R})$ is defined as minus one third of the trace of the shielding[8],

$$\text{NICS}(\mathbf{r_R}) = -\frac{1}{3}\left(\sigma_{xx}(\mathbf{r_R}) + \sigma_{yy}(\mathbf{r_R}) + \sigma_{zz}(\mathbf{r_R})\right) \tag{18}$$

NICS$(\mathbf{r_R})$ contains information about the current density vector $\mathbf{J}$, not only in the plane of interest $xy$, being parallel to the molecular plane, but also in the orthogonal planes $yz$ and $xz$. It is clear that using NICS$(\mathbf{r_R})$ for planar molecules introduces spurious effects arising from electron flow perpendicular to the molecular plane and not only in the plane of interest, being the molecular plane. Therefore, the average shielding should not be considered as a descriptor for aromaticity.

Since currents due to the cyclic $\pi$ electron delocalisation are induced primarily by the external magnetic field applied perpendicular to the ring, the out-of-plane component of the NICS tensor should contain the information most relevant for aromaticity evaluations. A novel NICS index was proposed, $\text{NICS}_{zz}$[50] based on the total contribution to the out-of-plane component of the NICS-tensor and successfully applied[36,51]. Whenever NICS is mentioned in the following discussion, $\text{NICS}_{zz}$ is implied. No distinction is made between $\sigma$ and $\pi$ contributions as this does not affect the described rank problems.

Relying only on equation 15, the matrix equation one needs to solve reduces to

$$\left[\boldsymbol{\sigma}_{zz}\right] = \frac{1}{B^{\text{ext}}} \frac{\mu_0}{4\pi} \begin{bmatrix} \mathbf{Y} & -\mathbf{X} \end{bmatrix} \begin{bmatrix} \mathbf{J}_x \\ \mathbf{J}_y \end{bmatrix} \tag{19}$$

allowing to compute the current density components in the $x$ and $y$ directions, $J_x(\mathbf{r_b})$ and $J_y(\mathbf{r_b})$, based on the information available in the NICS-values, $\text{NICS}_{zz}(\mathbf{r_R}) = -\sigma_{zz}(\mathbf{r_R})$. Note that $\mathbf{J}$ always refers to the total current density over all space.

## 3 Computational Details

The present research focuses on benzene as the prototypical aromatic molecule. The results obtained serve as proof of principle and can easily be extended to other anti-, non- and aromatic molecules. To obtain the molecular geometry the Gaussian 09 code[52] was used. Full geometry optimization was performed at the HF/6-311g(d) level, followed by analytical frequency calculations to ensure a true minimum (ie $N_{\text{Imag}} = 0$).

### 3.1 Ring current density maps

Current densities in the presence of an external magnetic field can be calculated via perturbation theory. The perturbation equations are well known[53], the magnetic properties vary however widely with the choice of origin of the vector potential. In the ipsocentric approach[28,54] applied here, known as CTOCD-DZ, calculation of total magnetic properties is reduced to the calculation of two first order perturbed wave functions, one with linear momentum and one with an angular momentum perturbation operator. The current density at a given point in molecular space is calculated with that point taken as the origin. Ipsocentric current density maps are calculated at the coupled perturbed Hartree-Fock level in the 6-311+g(d) basis, using the GAMESS-UK package[55] linked to SYSMO[56].

The plotting convention is that the current density is determined in a plotting plane at a fixed height of 1 Bohr above the molecular plane. Contours represent the magnitude, and arrows the 2D projection of the current density per unit inducing magnetic field. As the current density values, expressed in au, are rather small, the values are multiplied with a factor 20 in the plots. Aromaticity/antiaromaticity is diagnosed by observation of anticlockwise/clockwise circulations of induced ring current, corresponding to diatropic and paratropic ring currents, respectively.

The current density is obtained on two types of grids, a denser and a less dense one. The dense grid contains 56033 points at which the current density is calculated. Using this grid with the appropriate weights leads to a precision of 0.01 in the calculation of NICS-values. The less dense grid contains 5040 points, leading to a precision of 0.1 in the calculation of the NICS-values. In all cases the NICS computed as described above agree very well with GIAO[57] based values.

### 3.2 Shielding vector values, $\text{NICS}_{zz}(\mathbf{r_R})$ values

NICS is typically computed at ring centres (non weighted mean of the heavy atom coordinates). There is however a clear risk of extrapolating the global magnetic behaviour of one compound from just one single-value magnetic property (or a collection at the ring centres), as alluded to for instance by Lazzeretti et al.[9,58]. Therefore, distributions of NICS values around molecules have been widely employed to provide better insights in the overall molecular magnetic properties. NICS were evaluated at points above, and at grids in and around the molecule[41,59–61]. Alternatives for finite sets of NICS-measurements were suggested in more recent works[38,39,62].

In this research a selection of the grids proposed in literature is investigated. The precise grids are detailed below. NICS values are calculated from the Biot-Savart law as explained above. Although they can also be obtained from perturbation theory without direct reference to the current density[63], our approach has the advantage of more directly linking the current density to the NICS value.

### 3.3 Data fitting

Equation 19 boils down to a data fitting procedure. As this involves many more current density values than shielding vector values, this system has an infinite number of solutions. The solution presented in this work is the one with the least 2-norm solution, by applying singular value decomposition (SVD) to the underdetermined problem.

## 4 Results and discussions

The aim of the present paper is to examine carefully whether one can, in a robust manner, extract information on the current density map — the key characteristic for the aromatic behaviour of a molecule — from the NICS value(s) computed at one or more positions.

First of all, we will inspect NICS as formulated in equation 19. Can this value ever contain enough information about the underlying current density ? The almost intuitive way of interpreting the shielding vector is by making the translation towards its corresponding current density. Therefore, we inspect if shielding vector(s) ever allow to reconstruct the current density. If one can find several other current density fields that

give rise to the very same shielding vector, the validity of this "translation" disappears.

Finally, we will inspect the information content of a shielding vector, and we will exploit the noise in the information algebraically to show how different current density maps can give rise to the same shielding tensor. Furthermore, we will show that the different extensions of single NICS values to scans, surfaces etc. can be seen as attempts to reduce null spaces and thus reduce the concomitant noise. However, these attempts merely introduce a new set of rank problems.

### 4.1 The lack of information in $NICS_{zz}$

The original NICS corresponded to the average value of the diagonal elements of the shielding tensor. Later on, $NICS_{zz}$ became the preferred component. The first critical remark that can be made is that by using $NICS_{zz}$, one has to rely on equation 19 to retrieve information on the current density. However, this means that one never obtains information on the $z$-component of the current density vector. Table 1 summarises the maximum and minimum values for the $x, y$ and $z$ components of the ipsocentric current density vectors (in au) in benzene.

| | $J_x$ | | $J_y$ | | $J_z$ | |
|---|---|---|---|---|---|---|
| | max | min | max | min | max | min |
| $C_6H_6$ | 0.43 | -0.57 | 0.24 | -0.39 | 0.05 | -0.05 |

**Table 1** Maximal and minimal values for the current density components (expressed in au) for benzene in the integration grid using in SYSMO[56].

Although the values for the $z$-component of the current density are roughly tenfold smaller than the $x$ and $y$ counterparts, they still constitute a non-negligible part of the current density. One should thus be aware that whenever using only the $zz$ term of the shielding vector, being $NICS_{zz}$, one always ignores a non-zero term. From this point on, the full shielding vector will be investigated.

### 4.2 Is there a one-to-one correspondence between the shielding vector and the current density map?

In this section, the uniqueness of the current density map derived from a given shielding vector at one particular point in space is inspected for benzene. The values for the $x, y$ and $z$ components of the current density at the points of the dense grid are used in equation 16 in order to create the vector $\boldsymbol{\sigma}$ at several points of interest. Given the coordinates of the point at which the $\boldsymbol{\sigma}$ vector is calculated, $(x_R, y_R, z_R)$, and the set of points at which the components of $\mathbf{J}$ are calculated, $\{(x_b, y_b, z_b)\}$, the coordinate matrix $\mathbf{C}$ is created. Multiplication with the current density vector $\mathbf{J}$ generates the shielding vector $\boldsymbol{\sigma}$ at the coordinates requested. The values for $\boldsymbol{\sigma}$ obtained in this way at 1 Å above the centre of the ring are given in figure 1. This is a unique value as we go from a given grid of current density vectors via the law of Biot-Savart to $\boldsymbol{\sigma}$. The reverse could, in principle, also be suggested. This is perfectly well possible for an analytical expression where integration and differentiation are inverse operations. For the calculation of $\boldsymbol{\sigma}$, this is not what is done and extracting current density data from a single $\boldsymbol{\sigma}$ vector is obviously problematic. However, this is insufficiently well appreciated; hence we show here explicitly a few types of transformations in the current density that keep $\boldsymbol{\sigma}$ the same for drastically different current density maps.

Assume that we transform the coordinates of the grid at which the components of $\mathbf{J}$ are obtained as presented in expression 20, with $\phi$ an arbitrary scaling factor.

$$\begin{aligned} x_b &\rightarrow x_R(1-\phi)+\phi x_b \\ y_b &\rightarrow y_R(1-\phi)+\phi y_b \\ z_b &\rightarrow z_R(1-\phi)+\phi z_b \end{aligned} \tag{20}$$

It can then be seen that the distance matrix $\mathbf{C}$, equation 16 and 17, is scaled with a factor $\phi/(\sqrt{\phi^2})^3$. In order to obtain the same vector $\boldsymbol{\sigma}$, the vector $\mathbf{J}$ needs to be scaled with the factor $(\sqrt{\phi^2})^3/\phi$. Three possible current density fields are depicted in figure 1, derived for the $\sigma$-vector above the centre of the ring, at 1 Bohr. The scaling $\phi$ applied is 0.5 (a), 1(b) and 5(c). Note that this does not correspond to extracting a current density from $\boldsymbol{\sigma}$ data but is a direct scaling argument for the current density to show that infinitely many current densities may lead to the same $\boldsymbol{\sigma}$ vector.

Zooming in on the carbon skeleton shows the remarkable feature that one shielding vector can be associated with a counterclockwise, a clockwise ring current pattern and even a current density that can not be mapped to a ring current. One shielding vector can thus be generated from three completely different current densities (if one restricts the analysis to the neighbourhood of the carbon skeleton as is usually done): the regular aromatic flow, no current above the carbon atoms, and an anti-aromatic behaviour above the carbon skeleton. An infinite set of current density patterns results in the same shielding vector. Only one of them is the true ab initio one, but there is no guarantee that another behaviour could be concluded by the end-user, if he has no knowledge on the true current density. Establishing what is the true underlying ab initio current density from merely the current density data is (currently) intractable. This would require a full set of pure state, or even only ensemble $N$-representability constraints as they also occur for electron densities in Density (Matrix) Functional Theory and Variational Density Matrix methods[64]. Such con-

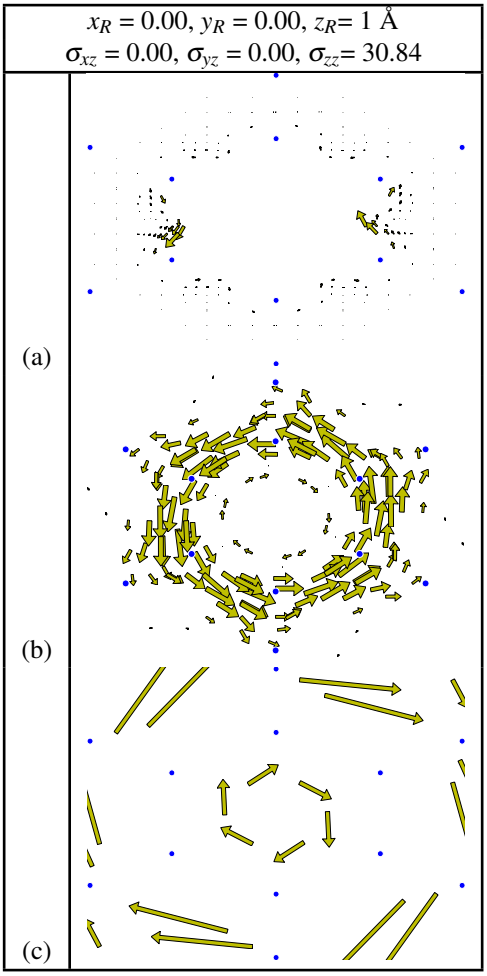


**Fig. 1** Three current density maps at a height of 1 Bohr above the plane that result in the same $\boldsymbol{\sigma}$ vector computed at 1 Å above the centre of the molecule.

straints for current densities are only being explored since recently[65]. Also note that the present transformation does not merely add a function that integrates to zero ($\int f(\mathbf{r})\mathrm{d}^3\mathbf{r} = 0$) in the integral form of the law of Biot-Savart:

$$\mathbf{B}^{\mathrm{ind}}(\mathbf{r_R}) = \frac{\mu_0}{4\pi}\int_{\mathbb{R}^3}\left[\frac{\mathbf{J}^B(\mathbf{r})\times\widehat{(\mathbf{r_R}-\mathbf{r})}}{|\mathbf{r_R}-\mathbf{r}|^2} + f(\mathbf{r})\right]\mathrm{d}^3\mathbf{r} \qquad (21)$$

### 4.3 Extracting a current density field from shielding vector data.

The above demonstration that different current densities can lead to the same $\boldsymbol{\sigma}$ vector is based on scaling arguments. In practice, most users compute NICS values and interpret these as reflecting a ring current of either aromatic, anti-aromatic or non-aromatic nature. Scaling arguments do not provide the sole demonstration of the ambiguity in the current density. If one uses $\boldsymbol{\sigma}$ vectors as information sources, there are also clear problems of algebraic nature. Equation 16 establishes the connection between the current density field and the $\boldsymbol{\sigma}$ vector. In practice, the dimension of the $\boldsymbol{\sigma}$ vector is much smaller than the grid on which the current density vectors are computed. This entails that the vector $\mathbf{C}$ is a non-rectangular matrix. The true information content of the shielding vector $\boldsymbol{\sigma}$ with respect to the current density vectors on the grid can be revealed by inspecting the null space of $\mathbf{C}$. In order to do so, the distance matrix is decomposed through the singular value decomposition (SVD). The SVD technique is an orthogonal decomposition of the $N \times N_b$ matrix that satisfies the following relationship:

$$\mathbf{C} = \mathbf{U}\Sigma\mathbf{V}^{\mathbf{T}} \qquad (22)$$

The matrices $\mathbf{U}$ and $\mathbf{V}$ are orthogonal matrices, spanning the orthogonal space of respectively the shielding vectors and the current density vectors.

Having for example one shielding vector ($\sigma_{xz}(\mathbf{r}_1)$, $\sigma_{yz}(\mathbf{r}_1)$, $\sigma_{zz}(\mathbf{r}_1)$) at the input of the problem, the distance matrix $\mathbf{C}$ has 3 singular values different from zero. Taking the dimension of the grid at which the current density vector is calculated as $N_b$, the null space has dimension $(3 * N_b - 3 \times 3 * N_b)$. The null space thus contains $(3 * N_b - 3)$ vectors $\{\mathbf{V}_i\}$ of dimension $N_b \times 1$ and these vectors can be added in any possible linear combination to the original vector $\mathbf{J}$ without affecting the shielding vector $\boldsymbol{\sigma}$. As such, the new vector $\mathbf{J}'$, constructed with a user-chosen vector of coefficients $\{d_i\}$

$$\mathbf{J}' = \mathbf{J} + \sum_{\mathbf{V}_i \in \mathrm{Null}(\mathbf{C})} d_i \mathbf{V}_i \qquad (23)$$

leads to the very same shielding vector, but with a completely different current density pattern.

To show this, we examine the effect of the null space for benzene. The SVD for very large matrices may become computationally quite demanding, which is why here we use the less dense current density grid. Note, however, that this does not affect the fundamental problem of the existence of a null space. On the contrary, using a denser grid would worsen the problem, i.e. increase the null space dimension. The ab initio current density for this less dense grid is given in figure 2(a). This current density gives rise to the shielding vector components given in figure 2(a) at 1 Bohr above the centre of the ring. Note that the change in grid has only a minor effect on these components. Any possible current density pattern that consists of the ab initio current density plus an arbitrary combination of vectors included in the null space yields the very same shielding vector. In the example of figure 2(b) a symmetry-projected combination of null space vectors is added to the ab initio current density. The impact is enormous: one is able to generate a ring current of opposite nature without affecting the $\boldsymbol{\sigma}$ vector. This means that two individuals may claim different conclusions from computed shielding tensors where none of these can be shown wrong. For molecules of lesser known nature than benzene, a dispute cannot be settled without actually computing the current density, making the latter a far superior aromaticity indicator.

### 4.4 Is there a solution for the problem of the lack of information?

As reported above, from the moment **C** has a non-trivial null space, the current density vector can be changed such that a different current density pattern can be obtained. This is a reconfirmation of the artefact in NICS already alluded on by Lazzeretti[9]. A naive way of eliminating this problem would then be to simply increase the number of points where the shielding tensor components are computed. This would reduce the dimension of the null space. Yet, as will be shown, the fact that computers have limited precision entails that other singularities will appear, much like what has been observed previously in the study of molecular electrostatic potentials[48]. It should therefore be inspected whether enlarging the sampling set allows to evolve towards the so-desired one to one relationship between a set of shielding vectors and the current density pattern. The problem with enlarging the set of points where shielding tensor components are computed is that points will need to be included that lie so close to each other that within computational precision they coincide. This leads to a rank reduction of the matrix and is reflected in singular values approaching zero. The condition number of a matrix is defined by the ratio of the largest ($s_{max}$) to the smallest ($s_{min}$) singular value. When the matrix is singular, containing exactly redundant information, the condition number is infinite. If the condition number is very large, the matrix is ill

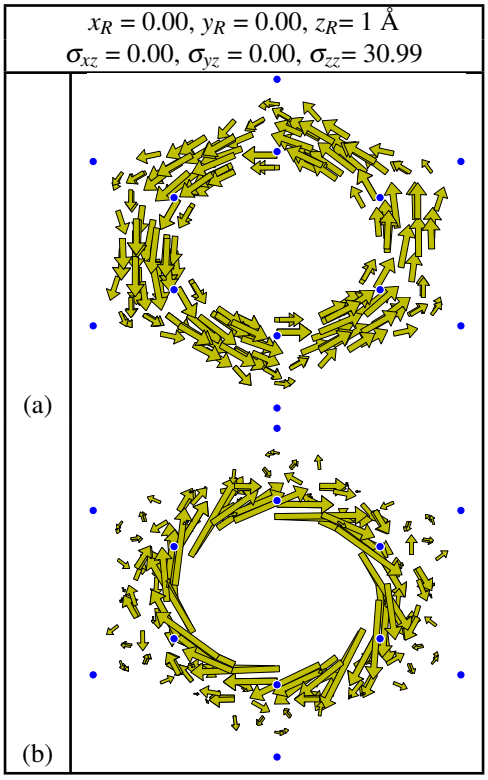


**Fig. 2** (a) Ab initio current density in benzene plotted in a plane 1 Bohr above the molecular plane and (b) a current density distribution obtained by addition of a symmetry adapted combination of null space vectors $\{\mathbf{V}_i\}$. Both current densities lead to exactly the same shielding tensor components.

| | $x_{\min}$ | $x_{\max}$ | $y_{\min}$ | $y_{\max}$ | $z_{\min}$ | $z_{\max}$ | $N_R$ |
|---|---|---|---|---|---|---|---|
| $G_{COM}$ | 0.0 | 0.0 | 0.0 | 0.0 | 1.89 | 1.89 | 1 |
| $G_{\parallel}$ | -5.0 | 5.0 | 0.0 | 0.0 | 1.89 | 1.89 | 11 |
| $G_{\perp}$ | 0.0 | 0.0 | 0.0 | 0.0 | 0.0 | 5.0 | 11 |
| $G^*_{\perp}$ | 0.0 | 0.0 | 0.0 | 0.0 | 0.1 | 5.0 | 50 |
| $G_{2D}$ | -5.0 | 5.0 | -5.0 | 5.0 | 1.89 | 1.89 | 121 |
| $G_R$ | -5.0 | 5.0 | -5.0 | 5.0 | 0.0 | 4.72 | 121 |
| $G^*_{2D}$ | -5.0 | 5.0 | -5.0 | 5.0 | 1.89 | 1.89 | 576 |
| $G_{3D}$ | -5.0 | 5.0 | -5.0 | 5.0 | 0.0 | 4.72 | 605 |

**Table 2** Grids used to compute shielding tensors on (see text), together with their dimension $N_R$ and range along three orthogonal directions (in Bohr).

conditioned and rank deficient. The rank of the matrix can be reduced by one for each singular value $s_i$ where the ratio $s_i/s_{max}$ is smaller than the precision of the data.

The central question therefore is twofold

1. Is it useful to enlarge the set of points where shielding tensors are computed, i.e. can one significantly reduce the null space ?

2. Can sufficient points be added or when do new singularities due to computer precision appear ?

Both questions can by answered by inspecting the behaviour of different shielding vector sampling proposals. Several grids of points where shielding tensors are computed will be investigated for benzene. Table 2 introduces the different grids used and details also their dimension $N_R$. $N_b$, the number of current density grid points used in SYSMO equals 15120 throughout. Several of the shielding tensor grids correspond to suggested grids in literature. A first grid ($G_{COM}$) contains only one point and corresponds to a point at 1 Å above the centre of the ring. A grid along a line parallel ($G_{\parallel}$) to the molecular plane at a height of 1.8897 Å along the longest axis of the molecule is also included.[39,66] as well as a grid consisting of a line perpendicular ($G_{\perp}$) to the molecular plane containing the centre-of-mass[38,62]. A plane parallel to the molecular plane at a height of 1 Å defines the ($G_{2D}$) grid and the $G_{3D}$ grid varies in three directions. A random set of points within a box of specified size is also used ($G_R$). The nature of grids labeled with $^*$ equals those without except that they contain a larger number of points $N_R$ to investigate the impact of changing this variable.

Each grid gives rise to a matrix **C** as in equation 16. Table 2 reports for every grid key characteristics. The full rank equals $3N_R$ and thus the number of shielding tensor components used. Besides the condition number, in analogy with the SVD analysis of Francl[48] for molecular electrostatic potentials, a SVD rank estimate is reported as the number of singular values for which the ratio of $s_i$ to $s_{\max}$ exceeds $10^{-8}$.

Each setting is characterised by its condition number and the subsequent SVD rank estimate. The full rank equals the number of shielding vector values that are used. In analogy with the SVD analysis of Francl[48], the SVD rank estimate is taken as the number of singular values for which the ratio of $s_i$ to $s_{\max}$ does not exceed $10^{-8}$. The condition number and the SVD rank estimate for each setting is summarised in table 3.

| | Full rank | Condition number | SVD rank estimate |
|---|---|---|---|
| $G_{COM}$ | 3 | 1.16 | 3 |
| $G_{\parallel}$ | 33 | $1.23 \times 10^1$ | 33 |
| $G_{\perp}$ | 33 | $1.54 \times 10^4$ | 33 |
| $G^*_{\perp}$ | 150 | $3.25 \times 10^{16}$ | 70 |
| $G_{2D}$ | 363 | $1.00 \times 10^2$ | 363 |
| $G_R$ | 363 | $4.31 \times 10^9$ | 347 |
| $G^*_{2D}$ | 1728 | $8.95 \times 10^{10}$ | 1586 |
| $G_{3D}$ | 1815 | $9.89 \times 10^5$ | 1815 |

**Table 3** Characteristics of the shielding vector grids.

Table 3 shows several important points. For instance, the condition number does not (solely) depend on the number of points where the NICS are computed. This is illustrated by the comparison of the condition numbers for the grids $G_{\perp}$ and $G_{\parallel}$. Both grids have the same value $N_R$ of 11 but the condition numbers are very different. $G_{\perp}$ is thereby a much worse grid and the practice of scanning NICS values along the line orthogonal to the ring plane is strongly advised against. Note also that increasing $N_R$ in this same type of grid and removing the in plane NICS point from the grid does not alleviate the problem. Instead, the $G^*_{\perp}$ grid results in a prototypical ill-conditioned problem. Introducing more points in the grid worsens the condition number significantly. This means that adding more points does not bring more information. This is confirmed by the SVD rank estimate. This estimate reflects what the *practical* rank is instead of the Full rank. Indeed, the full rank is not 150 but only 70. A near five-fold increase in number of NICS data merely doubles the practical rank.
The condition number for the $G_{2D}$ grid is not too bad but also here the mere addition of more points as in the $G^*_{2D}$ grid does not improve that much the characteristics of the grid. The 1728 NICS data points only lead to a practical rank of 1586 and moreover results in a dramatically bad condition number. The $G_{3D}$ grid performs comparatively better than the $G^*_{2D}$ one despite containing the same number of NICS data. This reveals that the number of points $N_R$ is far from all determining and rather a judicious choice of positions where to compute the shielding tensor components would seem to be more im-

portant. The conditional phrasing is appropriate as the fact still remains that there is a very large null space that remains. This fact is hidden from the condition number and SVD rank estimate as these do not use the exact zero singular values. Moreover, as one includes more data points to reduce the dimension of the null space, the SVD rank does not increase equally fast.

The $G_R$ grid is another example of a very poor grid. The condition number is very high and at the same time the SVD rank estimate reveals that there is much redundant information. The $G_{COM}$ grid, although with only one NICS grid point and thus a shielding vector of dimension 3, has an apparently better condition number but as it also has the largest null space, so it is also of little use.

At first glance, the $G_{\|}$ and $G_{2D}$ grids seem to serve best but the null space remains massive. One of the possible current density maps comes from the least-square SVD norm. The resulting current density maps for three different grids are presented in figure 3. They differ among each other and it is important to stress again that one can always add a combination of vectors from the null space to the current density.

The observations in table 3 for benzene are qualitatively similar among all molecules as they depend on the relative number of data points on the NICS versus current density grid.

Any chemist knows benzene is aromatic and a ring current inferring anti-aromaticity would be met with ridicule even though that current density pattern might give the same set of NICS data. However, for less obvious cases the situation is much less clear and the sole use of NICS indices is problematic. Different workers may come to different conclusions on the underlying current density and thus the degree of (anti-)aromaticity. Nevertheless, NICS is still of some use. As stated by Stanger[67,68], many chemists are not familiar with the analysis of vector fields and then quantities like NICS values can give useful information on some sort of strength of the current density. In any case, however, the NICS values should not be considered solely. First the current density, as obtained from an ab initio calculation, should be reported and analysed, possibly followed by key characteristics of the current density. NICS may be one such characteristic besides e.g., the highest magnitude of a current density vector passing through a bond intersecting plane[69–73]. Note also that the problem, illustrated here for the small molecule benzene, will grow larger for larger molecules where the current density is computed on larger grids to compute NICS values. The size of the grid on which the current densities is computed grows much quicker than the grid on which NICS data are computed, resulting in even larger null spaces. This adds to the problematic character of NICS in e.g., polycyclic compounds where it was earlier found that NICS do not convey information on local aromaticity[74–76].

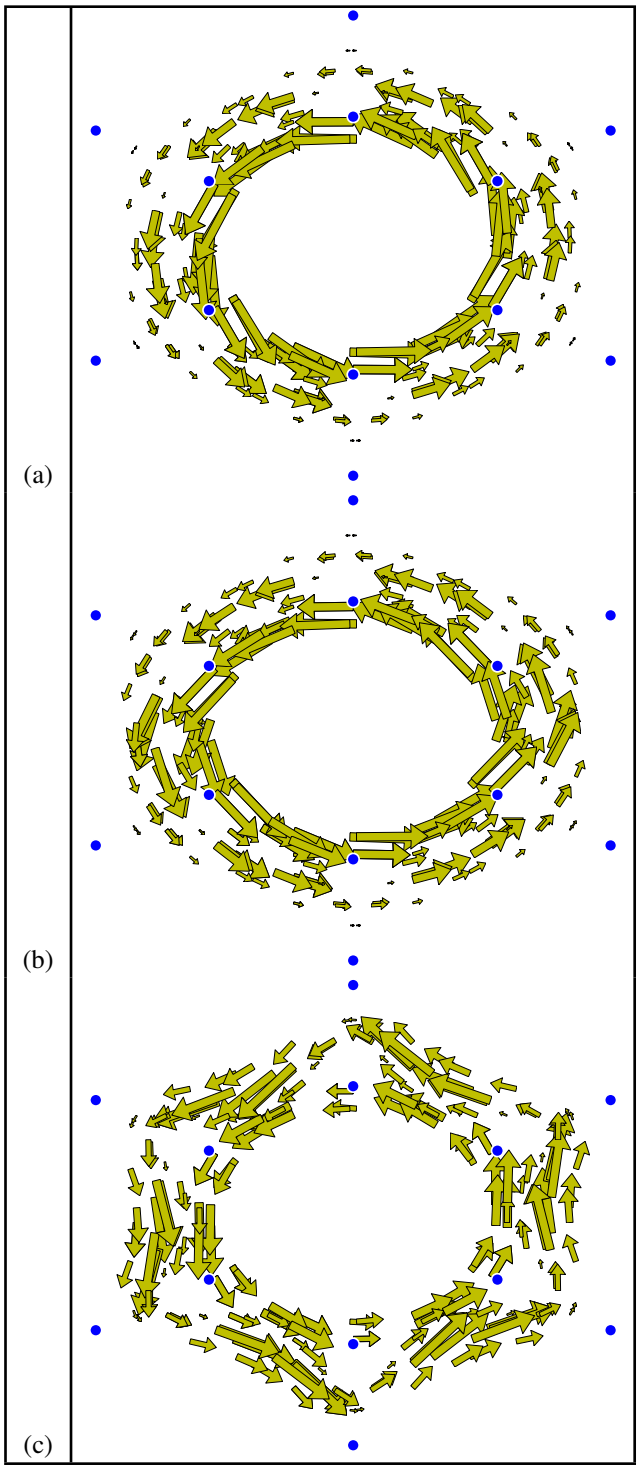


**Fig. 3** Least squares norm solution to SVD. The current density obtained from (a) the $G_{COM}$ grid, (b) a line parallel to the molecular plane at 1 Å above the molecular plane $G_{\|}$ and (c) the $G_{2D}$ grid

## 5 Conclusions

Nucleus independent chemical shifts (NICS) are among the most used indices to assess aromaticity of molecules, part due to their ease of calculation. However, it is important to realise that NICS rely on the integration of a (potentially) complicated pattern of induced ring currents —through the law of Biot-Savart— to a single number or a limited set of numbers on a grid of points. As the number of positions where the NICS are computed is usually much lower than the dimension of the grid on which current densities are calculated, it can be shown algebraically that for small numbers of NICS positions, one cannot reconstruct the underlying current density pattern. We have shown this explicitly for benzene by revealing different current density maps that yield the same NICS values. Extending the number of NICS positions to reduce the null space problems does not help due to the limited precision of computers which introduces a different type of rank problems.

Therefore, we advise not to use NICS-values as sole indices of aromaticity, but to rely on the inspection of current density maps to see whether a ring current exists and what its nature is. In this sense, one should replace the widespread current simple use of NICS or any other coarse-grain quantity by an inspection of the current density map *and*, if so desired, the reporting of the NICS value or the other coarse-grain quantity. A molecule can be considered as aromatic if careful and explicit reporting and studying of the current density pattern reveals a diatropic ring current, after which a NICS value may be given to reflect the current density in a condensed form. Reporting NICS values without at the same time showing the current density map is prone to error and to be avoided in all instances.

## 6 Acknowledgements

All authors are members of the QCMM alliance Ghent-Brussels and acknowledge financial support from the Research Foundation Flanders (FWO-Vlaanderen), G.A. as predoctoral fellow. The authors also acknowledge the Special Research Fund of Ghent University for continuous support. The computational resources (Stevin Supercomputer Infrastructure) and services used in this work were provided by the VSC (Flemish Supercomputer Center), funded by Ghent University, the Hercules Foundation, and the Flemish Government - department EWI. Kind assistance of Dr. Ward Poelmans is gratefully acknowledged. Dr. Amnon Stanger (Technion, Israel Institute of Technology) and Dr. Patrick Fowler (The University of Sheffield) are gratefully acknowledged for their useful suggestions.

## References

1 M. Faraday, *Philos. Trans. R. Soc. London*, 1825, **115**, 440–466.
2 L. Newell, *J. Chem. Educ.*, 1926, **3**, 1248–1253.
3 A. Kekulé, *Justus Liebigs Ann. Chem.*, 1857, **104**, 129–150.
4 A. Kekulé, *Bulletin de la Société Chimique de Paris*, 1865, **3**, 98–111.
5 A. Kekulé, *Justus Liebigs Ann. Chem.*, 1866, **137**, 129–196.
6 T. M. Krygowski, M. K. Cyranski, Z. Czarnocki, G. Hafelinger and A. R. Katritzky, *Tetrahedron*, 2000, **56**, 1783–1796.
7 M. K. Cyranski, T. M. Krogowski, A. R. Katritzky and P. V. R. Schleyer, *J. Org. Chem.*, 2002, **67**, 1333–1338.
8 P. V. R. Schleyer, C. Maerker, A. Dransfeld, H. J. Jiao and N. J. R. V. Hommes, *J. Am. Chem. Soc.*, 1996, **118**, 6317–6318.
9 P. Lazzeretti, *Phys. Chem. Chem. Phys.*, 2004, **6**, 217–223.
10 E. Steiner, P. W. Fowler and L. W. Jenneskens, *Angew. Chem., Int. Ed.*, 2001, **40**, 362–366.
11 R. Gershoni-Poranne and A. Stanger, *Chem. Soc. Rev.*, 2015, **44**, 6597–6615.
12 T. M. Krygowski and M. K. Cyranski, *Chem. Rev.*, 2001, **101**, 1385–1419.
13 C. F. Matta and J. Hernandez-Trujillo, *J. Phys. Chem. A*, 2003, **107**, 7496–7504.
14 J. Poater, X. Fradera, M. Duran and M. Sola, *Chem. - Eur. J.*, 2003, **9**, 400–406.
15 E. Matito, M. Duran and M. Sola, *J. Chem. Phys.*, 2005, **122**, 014109.
16 P. Bultinck, R. Ponec and S. Van Damme, *J. Phys. Org. Chem.*, 2005, **18**, 706–718.
17 P. Bultinck, M. Rafat, R. Ponec, R. Carbó-Dorca, B. van Gheluwe and P. L. A. Popelier, *J. Phys. Chem. A*, 2006, **110**, 7642–7648.
18 J. Poater, M. Duran, M. Sola and B. Silvi, *Chem. Rev.*, 2005, **105**, 3911–3947.
19 K. Jug and A. M. Koster, *J. Phys. Org. Chem.*, 1991, **4**, 163–169.
20 A. R. Katritzky, M. Karelson, S. Sild, T. M. Krygowski and K. Jug, *J. Org. Chem.*, 1998, **63**, 5228–5231.
21 A. Katritzky, P. Barczynski, G. Musumarra, D. Pisano and M. Szafran, *J. Am. Chem. Soc.*, 1989, **111**, 7–15.
22 J. Poater, I. Garcia-Cruz, F. Illas and M. Sola, *Phys. Chem. Chem. Phys.*, 2004, **6**, 314–318.
23 P. Bultinck, *Faraday Discuss.*, 2007, **135**, 347–365.
24 A. Stanger, *Chem. Commun.*, 2009, 1939–1947.
25 F. London, *J. Phys. Radium*, 1937, **8**, 397–409.
26 J. A. Pople, *Proc. R. Soc. London, Ser. A*, 1957, **239**, 541–549.
27 T. A. Keith and R. F. W. Bader, *Chem. Phys. Lett.*, 1993, **210**, 223–231.
28 P. Lazzeretti, M. Malagoli and R. Zanasi, *Chem. Phys. Lett.*, 1994, **220**, 299–304.
29 D. Geuenich, K. Hess, F. Kohler and R. Herges, *Chem. Rev.*, 2005, **105**, 3758–3772.
30 V. Minkin, M. Glukhovtsev and B. Simkin, *Aromaticity and Antiaromaticity: Electronic and Structural Aspects*, Wiley, 1994.
31 V. Elser and R. C. Haddon, *Nature*, 1987, **325**, 792–794.
32 P. Lazzeretti, *Prog. Nucl. Magn. Reson. Spectrosc.*, 2000, **36**, 1–88.
33 J. Aihara, *Chem. Phys. Lett.*, 2002, **365**, 34–39.
34 J. Poater, M. Sola, R. Viglione and R. Zanasi, *J. Org. Chem.*, 2004, **69**, 7537–7542.
35 Z. Chen, C. Wannere, C. Corminboeuf, R. Puchta and P. Schleyer, *Chem. Rev.*, 2005, **105**, 3842–3888.
36 H. Fallah-Bagher-Shaidaei, C. Wannere, C. Corminboeuf, R. Puchta and P. Schleyer, *Org. Lett.*, 2006, **8**, 863–866.
37 *Faraday Discuss.*, 2007, **135**, 367–401.
38 A. Stanger, *J. Org. Chem.*, 2006, **71**, 883–893.
39 R. Gershoni-Poranne and A. Stanger, *Chem. - Eur. J.*, 2014, **20**, 5673–5688.

40 P. V. R. Schleyer, M. Manoharan, Z. X. Wang, B. Kiran, H. Jiao, R. Puchta and van Eikema H. N. J. R., *Org. Lett.*, 2001, **3**, 2465–2468.

41 S. Klod and E. Kleinpeter, *J. Chem. Soc., Perkin Trans. 2*, 2001, **10**, 1893–1898.

42 G. Merino, T. Heine and G. Seifert, *Chem. - Eur. J.*, 2004, **10**, 4367–4371.

43 J. Juselius and D. Sundholm, *Phys. Chem. Chem. Phys.*, 1999, **1**, 3429–3435.

44 C. Foroutan-Nejad, S. Shahbazian, F. Feixas, P. Rashidi-Ranjbar and M. Sola, *J. Comput. Chem.*, 2011, **32**, 2422–2431.

45 S. Pelloni and P. Lazzeretti, *J. Phys. Chem. A*, 2011, **115**, 4553–4557.

46 S. Pelloni, G. Monaco, P. Lazzeretti and R. Zanasi, *Phys. Chem. Chem. Phys.*, 2011, **13**, 20666–20672.

47 S. Pelloni and P. Lazzeretti, *J. Phys. Chem. A*, 2013, **117**, 9083–9092.

48 M. M. Francl and L. E. Chirlian, *Reviews in Computational Chemistry*, John Wiley and Sons, Inc., 2007, pp. 1–31.

49 M. Alonso and J. Finn, *Physics*, Pearson Prentice Hall, 1992.

50 I. Cernusak, P. W. Fowler and E. Steiner, *Mol. Phys.*, 2000, **98**, 945–953.

51 C. Corminboeuf, T. Heine, G. Seifert, P. V. R. Schleyer and J. Weber, *Phys. Chem. Chem. Phys.*, 2004, **6**, 273–276.

52 M. J. Frisch, G. W. Trucks, H. B. Schlegel, G. E. Scuseria, M. A. Robb, J. R. Cheeseman, G. Scalmani, V. Barone, B. Mennucci, G. A. Petersson, H. Nakatsuji, M. Caricato, X. Li, H. P. Hratchian, A. F. Izmaylov, J. Bloino, G. Zheng, J. L. Sonnenberg, M. Hada, M. Ehara, K. Toyota, R. Fukuda, J. Hasegawa, M. Ishida, T. Nakajima, Y. Honda, O. Kitao, H. Nakai, T. Vreven, J. A. Montgomery, Jr., J. E. Peralta, F. Ogliaro, M. Bearpark, J. J. Heyd, E. Brothers, K. N. Kudin, V. N. Staroverov, R. Kobayashi, J. Normand, K. Raghavachari, A. Rendell, J. C. Burant, S. S. Iyengar, J. Tomasi, M. Cossi, N. Rega, J. M. Millam, M. Klene, J. E. Knox, J. B. Cross, V. Bakken, C. Adamo, J. Jaramillo, R. Gomperts, R. E. Stratmann, O. Yazyev, A. J. Austin, R. Cammi, C. Pomelli, J. W. Ochterski, R. L. Martin, K. Morokuma, V. G. Zakrzewski, G. A. Voth, P. Salvador, J. J. Dannenberg, S. Dapprich, A. D. Daniels, . Farkas, J. B. Foresman, J. V. Ortiz, J. Cioslowski and D. J. Fox, *Gaussian09 Revision D.01*, Gaussian Inc. Wallingford CT 2009.

53 G. Diercksen and R. McWeeny, *J. Chem. Phys.*, 1966, **44**, 3554–3560.

54 E. Steiner and P. W. Fowler, *J. Phys. Chem. A*, 2001, **105**, 9553–9562.

55 M. F. Guest, I. J. Bush, H. J. J. Van Dam, P. Sherwood, J. M. H. Thomas, J. H. Van Lenthe, R. W. A. Havenith and J. Kendrick, *Mol. Phys.*, 2005, **103**, 719–747.

56 *SYSMO Package: P. Lazzeretti and R. Zanasi (University of Modena, 1980) with additional routines for evaluation and plotting of current density by E. Steiner and P. W. Fowler, R. W. A. Havenith and A. Soncini.*

57 R. Ditchfield, *Mol. Phys.*, 1974, 789–807.

58 R. Carion, V. Liegeois, B. Champagne, D. Bonifazi, S. Pelloni and P. Lazzeretti, *J. Phys. Chem. Lett.*, 2010, **1**, 1563–1568.

59 P. V. R. Schleyer, M. Manoharan, Z. X. Wang, B. Kiran, H. J. Jiao, R. Puchta and N. J. R. V. Hommes, *Org. Lett.*, 2001, **3**, 2465–2468.

60 S. Klod, A. Koch and E. Kleinpeter, *J. Chem. Soc. Perkin Trans. 2*, 2002, 1506–1509.

61 E. Kleinpeter and S. Klod, *J. Mol. Struct.*, 2004, **704**, 79–82.

62 A. Stanger, *J. Org. Chem.*, 2010, **75**, 2281–2288.

63 M. Kaupp, *Calculation of NMR and EPR Parameters*, Wiley-VCH Verlag, 2004, pp. 293–306.

64 A. J. Coleman and V. I. Yukalov, *Reduced Density Matrices: Coulsons Challenge*, Springer-Verlag, 2000.

65 E. Tellgren, S. Kvaal and T. Helgaker, *Phys. Rev. A: At., Mol., Opt. Phys.*, 2014, **89**, 012515.

66 M. Schaffroth, R. Gershoni-Poranne, A. Stanger and U. Bunz, *J. Org. Chem.*, 2014, **79**, 11644–11650.

67 A. Stanger, The chemical bonds at the 21st century, 2015.

68 R. Gershoni-Poranne and A. Stanger, *Chem. Soc. Rev.*, 2015, **44**, 6597–6615.

69 H. Fliegl, D. Sundholm, S. Taubert, J. Juselius and W. Klopper, *J. Phys. Chem. A*, 2009, **113**, 8668–8678.

70 G. Monaco, R. Zanasi, S. Pelloni and P. Lazzeretti, *J. Chem. Theory Comput.*, 2010, **6**, 3343–3351.

71 A. Soncini, A. M. Teale, T. Helgaker, F. De Proft and D. J. Tozer, *J. Chem. Phys.*, 2008, **129**, 074101.

72 S. Radenkovic and P. Bultinck, *J. Phys. Chem. A*, 2011, **115**, 12493–12502.

73 S. Radenkovic, J. Durdevic and P. Bultinck, *Phys. Chem. Chem. Phys.*, 2012, **14**, 14067–14078.

74 S. Fias, S. Van Damme and P. Bultinck, *J. Comput. Chem.*, 2008, **29**, 358–366.

75 S. Fias, P. Fowler, J. Delgado, U. Hahn and P. Bultinck, *Chem. - Eur. J.*, 2008, **14**, 3093–3099.

76 S. Fias, S. Van Damme and P. Bultinck, *J. Comput. Chem.*, 2010, **31**, 2286–2293.

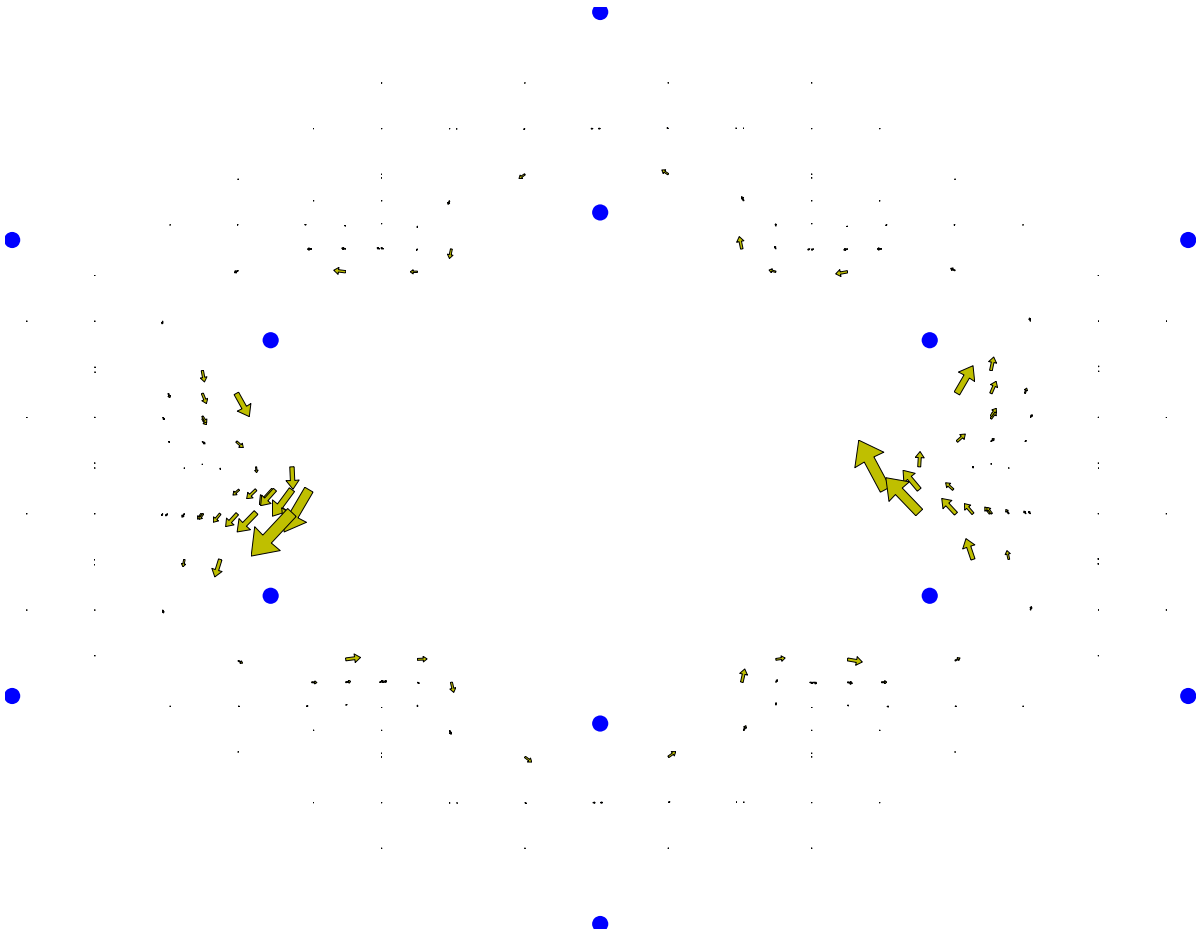

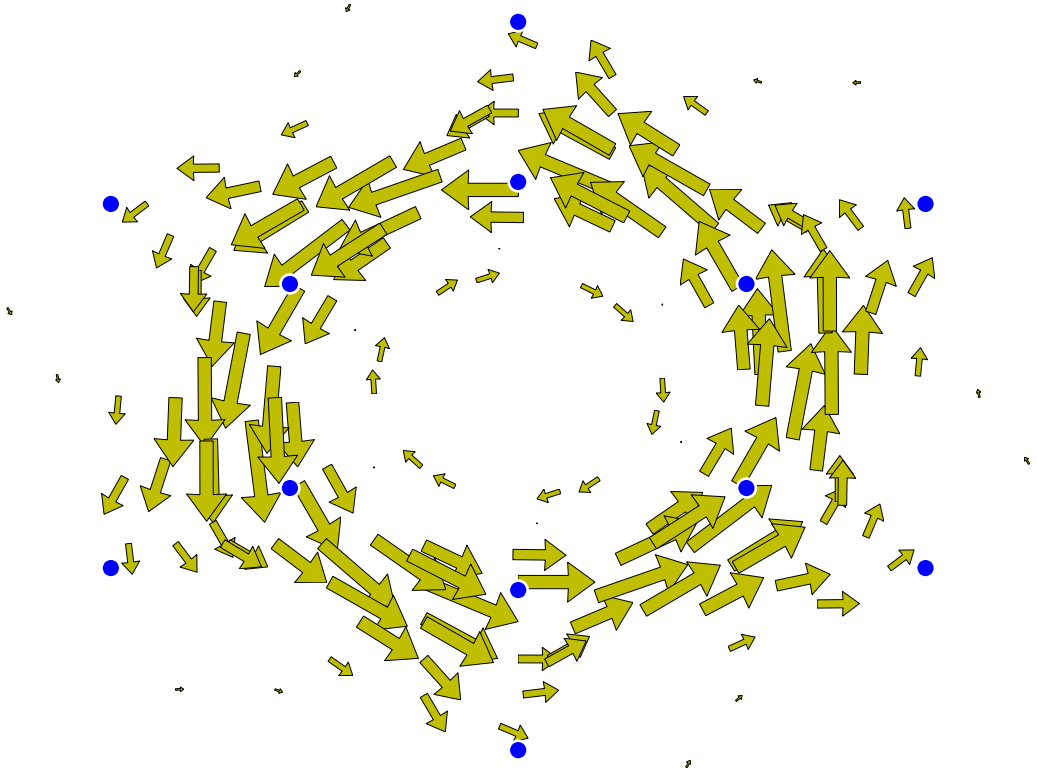

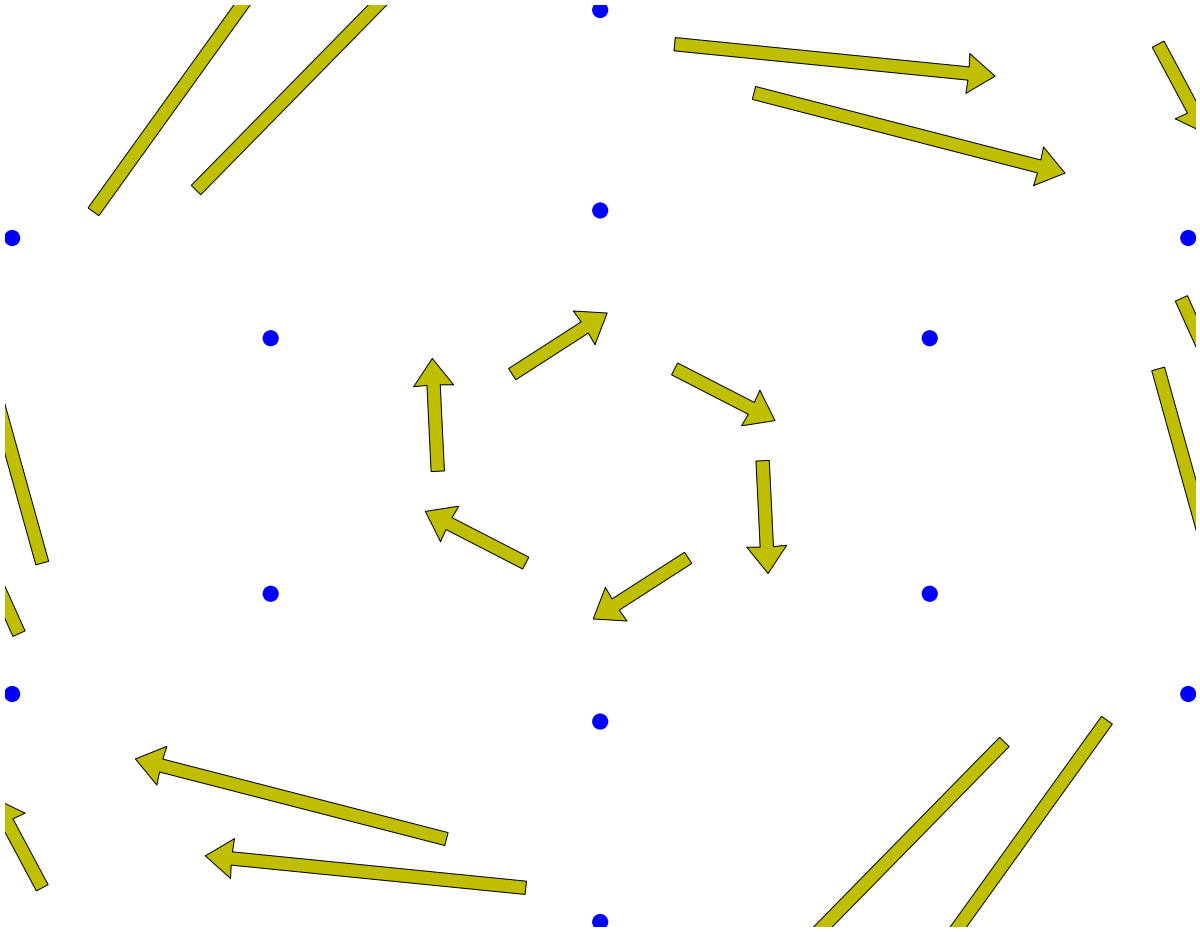

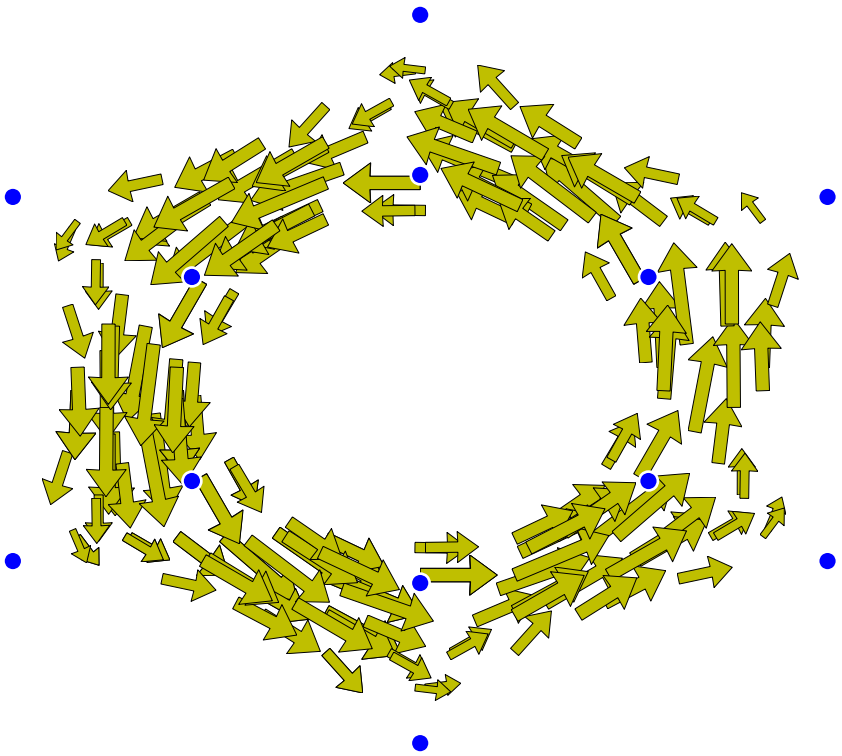

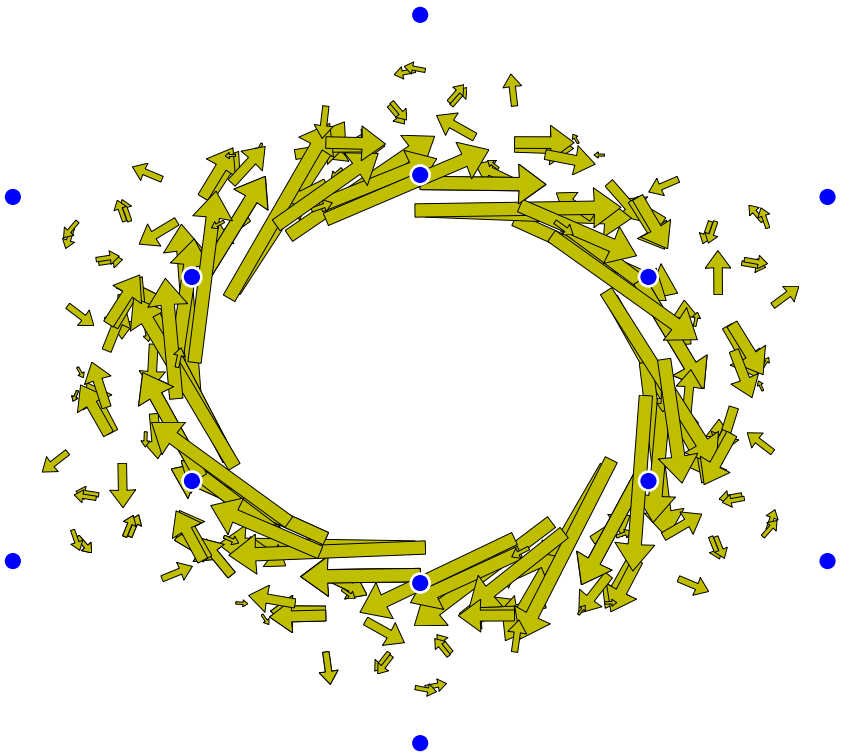

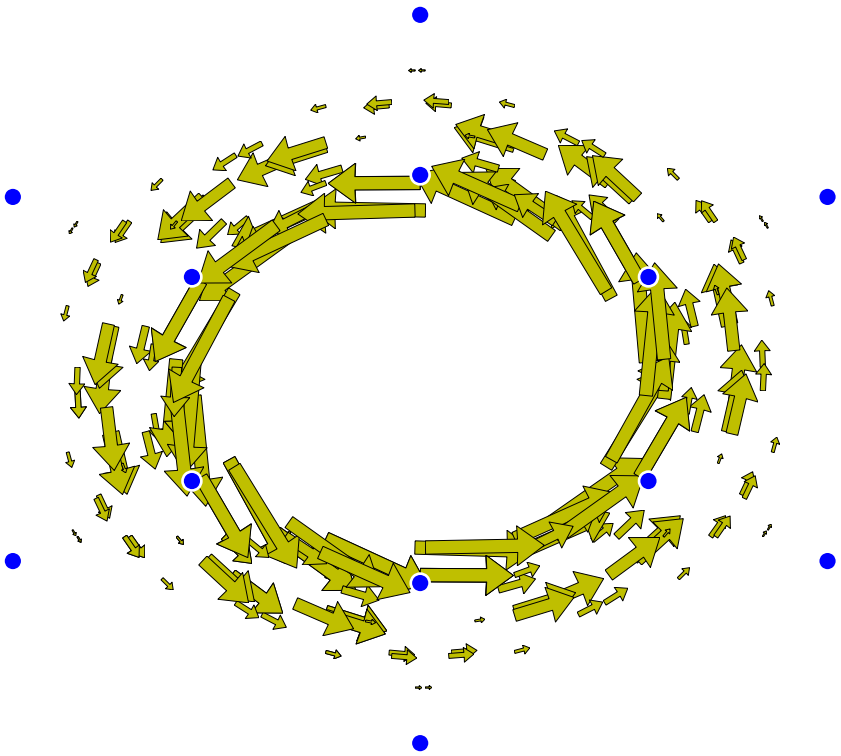

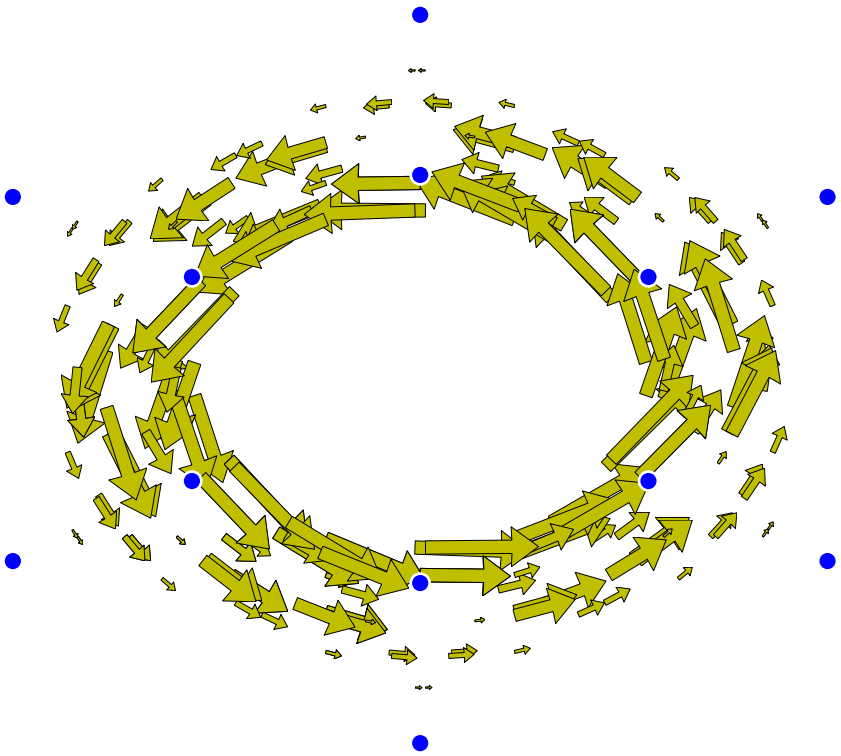

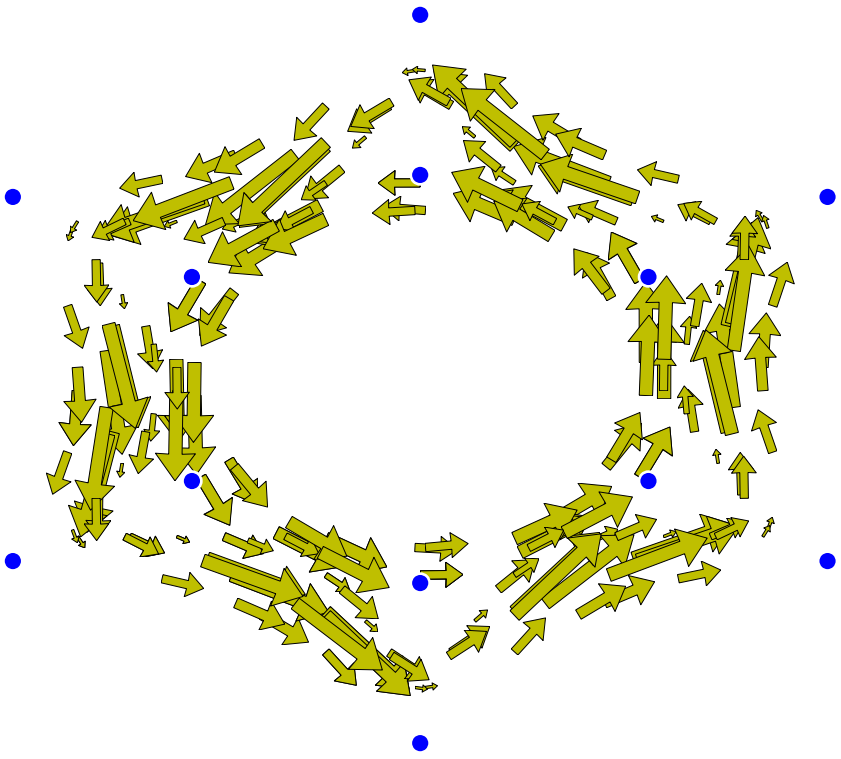

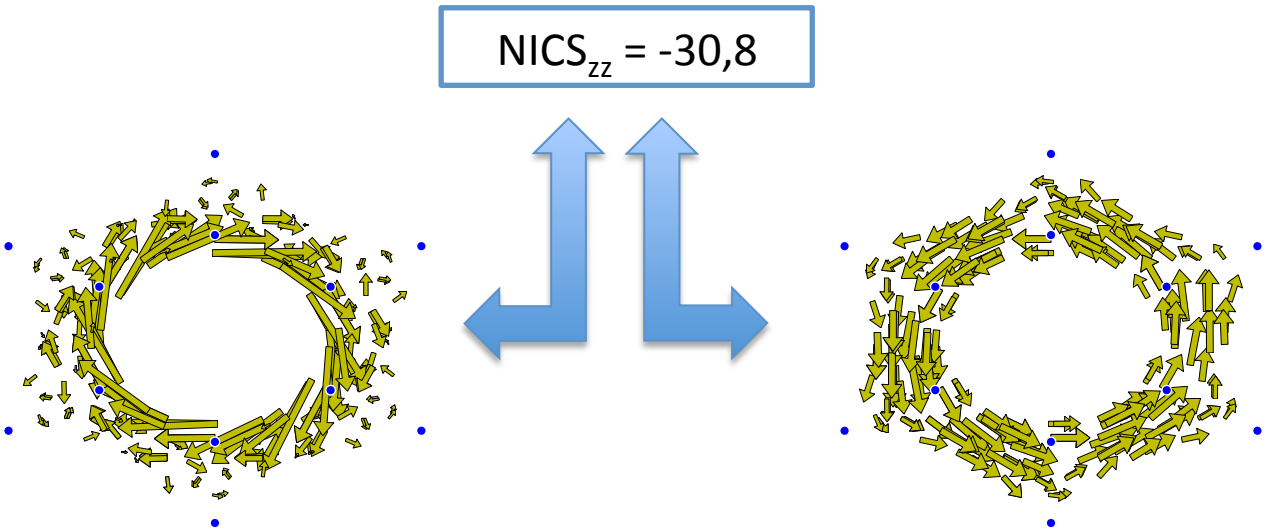


It is shown that no unique current density topology can be obtained from (sets of) NICS values.

Therefore, the use of NICS indices as aromaticity indices without prior analysis of the current density map is strongly discouraged